Water Resources Management (2025) 39:1055–1072
https://doi.org/10.1007/s11269-024-04005-5

Shear Layer Development and Fully Developed Flows in Compound Channels

João N. Fernandes[1,2] · **João B. Leal**[2] · **António H. Cardoso**[2,3]

Received: 8 September 2022 / Accepted: 7 October 2024 / Published online: 16 October 2024

Abstract
In alluvial river reaches, flood events are characterized by the inundation of the adjacent land near the main channel course. In these compound channel or overbank configurations, the flow structure is much more complex than in a single channel due to interactions between faster and deeper flow in the main channel and the slower and shallower flow in the lateral floodplains. Moreover, the interactions may be enhanced by the floodplain roughness as this region is usually covered by vegetation. The present study aims at understanding the streamwise flow development and the turbulent flow structure in such conditions. An experimental campaign was carried out in a laboratory compound channel. An iterative procedure to obtain the uniform flow was followed by successive change of the discharge distribution and downstream levels. In total, nine uniform flows were studied, namely (i) six with floodplains made of polished concrete and (ii) three with synthetic grass covering the floodplains. The boundary and mixing layers are presented and the effects of the shallowness and of the floodplain roughness on main flow mechanisms are assessed.

Keywords Compound channel · Vegetation · Turbulence, Mixing layer, Overbank flow

✉ João N. Fernandes
jnfernandes@lnec.pt

✉ João B. Leal
joao.leal@uia.no

✉ António H. Cardoso
antonio.cardoso@tecnico.ulisboa.pt

[1] Hydraulics and Environment Department, National Laboratory of Civil Engineering, Lisbon, Portugal

[2] Faculty of Engineering and Science, Universitetet i Agder, Kristiansand, Norway

[3] CERIS and DECivil, Instituto Superior Técnico, Lisbon University, Lisbon, Portugal

1 Introduction

During flood events the increase of the total conveyance of rivers is achieved with the inundation of the surrounding fields. As a result of the frequent occupation of the floodplains, this phenomenon can be a serious threat to population, environment and goods. When this overbank or compound channel flow occurs, important interactions between the faster flow in the main channel and the slower flow in the floodplains are observed. These interactions imply the exchange of mass and momentum among the flows, controlled by the mixing layer formed near the interface. Previous studies identified velocity gradient between the flows in main channel and floodplains (herein called sub-sections) as one of the main influential factors of interfacial large-scale vortices with vertical axis (e.g. Nezu et al. 1999).

In these overbank flows, the discharge for a given flow depth is much more difficult to predict than in single channels and several methods were developed to overcome this issue (Bousmar et al. 2016; Rahimi et al. 2022). Analytical solutions to predict the conveyance of compound channel were developed by Zeng et al. (2012) who identified the friction factor as the main influencing parameter and the much smaller effect of the dimensionless eddy viscosity on the precision of predictions.

To understand the development of the mixing layer between flows with different velocities, several studies have been developed over the last decades (e.g. Yule 1972). Chu et al. (1991) pointed out the importance of knowing the lateral spreading of the mixing layer as well as the stabilizing influence of the bottom friction. Booij and Tukker (2001) associated the width of the mixing layers with the development of the coherent structures responsible for the lateral momentum transfer.

Depending on the water depth, plane (or free) and shallow water mixing layers can be observed. In plane mixing layers, the velocity gradient between two streams is a source of turbulent kinetic energy and two-dimensional turbulent structures are generated. Further downstream, these structures become unstable and disintegrate into three-dimensional turbulence.

In shallow flows, three types of mixing layers can be generated namely (i) flows in straight channel with lateral roughness changes; (ii) confluences of flows with different velocities and (iii) compound channel flows (Vermaas et al. 2011).

For the study of the shallowness effect on the development of mixing layers, Uijttewaal and Booij (2000) carried out two experiments in a single channel where two flows with different velocities interacted. The bottom friction was found to affect the streamwise development of the mixing layer due to two factors, namely the decrease of the velocity gradient and the suppression of the Kelvin-Helmholtz instabilities that govern the spreading of that layer. For higher discharges, the mixing layer behaves as a plane mixing layer and self-similarity is maintained.

Depending on the flow characteristics, Booij and Tukker (2001) identified three regions in the longitudinal development of shallow-water mixing layers. In the first region, the width of the layer is smaller than the water depth and the influence of the bottom on the mixing layer is weak. In this region, the flow develops as a free mixing layer, but the bottom turbulence can slightly increase the initial spreading rate. In the second region, the bottom friction has a major influence on the development of the mixing layer, leading to a decrease of its spreading rate. Here, horizontal large-scale eddies develop with dimensions larger than the water depth. In the third region, these macro-vortices display horizontal dimensions

much larger than the water depth. The stabilizing influence of the bottom friction suppresses the generation of new large-scale eddies, leading to the equilibrium of the mixing layer.

Stocchino and Brocchini (2010) carried out velocity measurements in the water surface of a compound channel flow using Particle Image Velocimetry (PIV). The transverse gradient of the bottom elevation in compound channels was considered as the main factor for the generation of the horizontal macro-vortices. The water depth difference near the interface can sustain the generation of macro-vortices. Stocchino and Brocchini (2010) found that, for low relative depths (h_r, ratio between floodplain and main channel flow depths), $h_r <$ 0.33, the typical size of these vortices, generated near the interface, is independent of the streamwise coordinate as soon as the flow is fully developed. This suggests the importance of the topographic forcing which is not present in plane mixing layers.

Despite the extensive study of the flow characteristics in compound channels in both laboratory (e.g. Proust et al. 2016; Vojoudi Mehrabani et al. 2020; Prasad et al. 2022) and field (e.g. Myers and Lyness 1994), issues related to the longitudinal development of the interaction between the flows in main channel and floodplain and the characteristics of the mixing layer and scales are not fully studied.

In this work, the flow development in the longitudinal direction of a compound channel and the corresponding mixing layer width will be analysed. In the present compound channel experiments, downstream the initial separating plates of the main channel and the floodplains, in cross-section $x=0$ m, the flows in main channel and floodplains start to interact with each other and a mixing layer develops. The interaction of two flows with different velocities implies the exchange of mass and momentum among them. The mixing layer between the flows controls this exchange, which may include pollutants or sediments. After the verification of the boundary layer development in the centre of the main channel, for one flow case, the longitudinal evolution of the mixing layer width and the streamwise velocity and lateral shear stress will be analysed. For this propose, velocity measurements in four cross-sections are evaluated for six uniform flows: (i) three on floodplains made of polished concrete and (ii) three on synthetic grass covering the floodplains. Furthermore, the fully developed flows will be discussed for nine uniform flows.

2 Experimental Details

2.1 Experimental Setup and Instrumentation

The experimental campaign took place in a 10.0 m long and 2.0 m wide symmetrical and straight compound channel located at the National Laboratory for Civil Engineering (LNEC). The cross-section comprised two lateral rectangular floodplains (floodplain width, B_{fp} = 0.7 m) and one trapezoidal and central main channel (bank full height, h_b = 0.1 m, main channel width, B_{mc} = 0.6 m, and 45° lateral bank slope, s_y = 1). The cross-section of the compound channel is presented in Fig. 1, where h_{mc} and h_{fp} stand for the main channel and the floodplain flow depths, respectively.

The channel bottom was made of polished concrete and its longitudinal slope was s_0=0.0011 m/m. Six experiments were performed for the original polished concrete bottom (herein called *smooth boundary*), while three experiments were conducted with synthetic grass on the floodplains (*rough boundary*). Preliminary tests in a single channel were carried

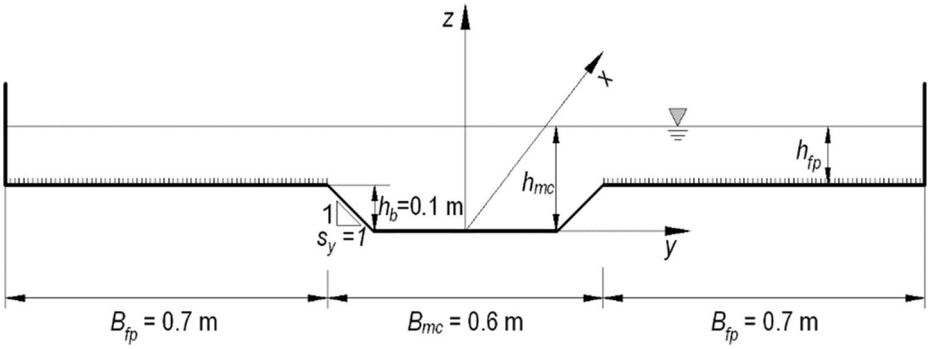

Fig. 1 Schematic representation of the compound channel

out to characterize the bed roughness resulting Manning's coefficient, $n=0.0092$ m$^{-1/3}$s for polished concrete and $n=0.0172$ m$^{-1/3}$s for synthetic grass.

Following the recommendation of Bousmar et al. (2005), separated inlets for the main channel and for the floodplains were installed. For each subsection, the incoming flow discharge was controlled with a valve and monitored through an electromagnetic flow meter with the accuracy of ±0.1 l/s. At the downstream end of the flume, independent tailgates for each subsection were used to adjust the water levels in the flume.

Water surface levels were measured with a point gauge (with an accuracy of ±0.1 mm) in 9 cross-sections at 12 lateral positions per cross-section.

Velocity measurements were carried out with a side looking Acoustic Doppler Velocimeter (ADV-vectrino). The acquisition time was fixed in 3 min at each measuring position, at a sampling frequency of 100 Hz. The velocity data were despiked with the filter of Goring and Nikora (2002). Only correlations and SNR higher than 70% and 15 dB, respectively, were considered. To align the ADV probe with the longitudinal direction, the pitch angle was slightly modified to get a depth averaged transverse velocity, V, equal to 0 near the floodplain sidewall. This correction was considered in the computation of the local mean velocity and the velocity fluctuations.

2.2 Experimental Procedure, Flow Cases and Control Variables

The longitudinal development of the compound channel flow and the corresponding boundary and mixing layers were analysed. For this purpose, velocity measurements were performed in several cross-sections.

Since, for a given flow depth, the subsection discharge distribution corresponding to uniform flow was not known a priori, an iterative procedure was followed to impose it at $x=0$ m (cf. Fernandes et al. 2018). The experimental conditions are listed in Table 1, where, apart from the variables previously defined, Q_{mc} and Q_{fp} are the main channel and the floodplain discharges, respectively, and $h_r = h_{fp}/h_{mc}$ stands for the relative flow depth.

The reference of each experiment (first column of Table 1) is to be read as: "*hr*" followed by "relative depth in percentage" and by "s" or "r" (for smooth and rough floodplains, respectively). Froude numbers are presented per subsection, $Fr_i = U_i/\sqrt{gR_i}$, where U is the cross-sectional average velocity, R is the hydraulic radius and subscript i stands for either main channel, *mc*, or floodplain, *fp*. The flow is subcritical for all tests, which is con-

Table 1 Experimental flow conditions

Flow case reference	h_{mc} (m)	h_r (–)	Q_{mc} ($l.s^{-1}$)	Q_{fp} ($l.s^{-1}$)	Q ($l.s^{-1}$)	U_{mc} ($m.s^{-1}$)	U_{fp} ($m.s^{-1}$)	Re_{mc} ($x10^{-5}$)	Re_{fp} ($x10^{-5}$)	Fr_{mc} (–)	Fr_{fp} (–)	Measurements Cross-sections, x (m)
hr010s	0.1119	0.11	34.9	3.3	38.2	0.61	0.20	2.02	0.09	0.67	0.58	7.5
hr015s	0.1172	0.15	38.8	6.0	44.8	0.64	0.25	2.25	0.17	0.69	0.61	1.1, 3.0, 5.0, 7.5
hr020s	0.1220	0.19	42.2	11.2	53.4	0.67	0.36	2.45	0.31	0.70	0.78	1.1, 3.0, 5.0, 7.5
hr025s	0.1309	0.24	46.7	18.6	65.3	0.68	0.43	2.71	0.50	0.69	0.80	7.5
hr030s	0.1402	0.29	54.2	26.4	80.6	0.72	0.46	3.17	0.66	0.70	0.76	1.1, 3.0, 5.0, 7.5
hr038s	0.1600	0.38	67.8	50.5	118.3	0.79	0.60	3.93	1.32	0.71	0.82	7.5
hr015r	0.1192	0.15	35.1	3.7	38.8	0.57	0.14	2.04	0.10	0.61	0.32	1.1, 3.0, 5.0, 7.5
hr020r	0.1244	0.21	39.3	7.3	46.6	0.61	0.21	2.28	0.20	0.63	0.44	1.1, 3.0, 5.0, 7.5
hr030r	0.1450	0.31	42.3	16.6	58.9	0.55	0.26	2.45	0.44	0.52	0.41	1.1, 3.0, 5.0, 7.5

sistent with the use of three independent downstream gates to control the flow depth in each subsection. The Reynolds number, $Re = 4U_iR_i/\nu$, where ν is the kinematic viscosity, is also included in Table 1.

After verifying the symmetry of the flow conditions, only half of the cross-section was investigated. In the half cross-section, the measuring mesh comprised 22 measuring verticals, 3 measuring points per vertical in the floodplain (between $0.4h_{fp}$ and $0.8h_{fp}$) and 7 in the main channel (between $0.10h_{mc}$ and h_b+$0.8h_{fp}$).

For most flow cases, the velocity measurements were conducted in cross-sections x=1.1 m, 3.0 m, 5.0 m and 7.5 m from the inlet section. As presented in Table 1, for flow cases hr01s, hr020s and hr038s, only cross-section at x=7.5 m was surveyed. Whenever additional measurements were made in specific points, they were referred in the text.

3 Streamwise Flow Development

3.1 Boundary Layer

Near fixed walls, the flow velocity increases from zero at the wall to a value that, in the case of unbounded-layer flows, corresponds to external frictionless flow (Schlichting 1968). In open-channels, fully developed flows are reached when this boundary layer occupies the entire flow depth.

The development of the boundary layer was assessed in the centre of the main channel for the flow case hr30s. For that purpose, vertical profiles of the streamwise velocity were measured in six cross-sections. The results are presented in Fig. 2, where the logarithmic-law profile $u\,(z)\,/u^* = 1/k\ln\,(zu^*/\nu\,) + 5.1$, where $\overline{u}\,(z)$ is the time-averaged velocity at elevation z, u^* is the friction velocity and k is the von Kármán constant (0.4), is also plotted (doted lines).

The streamwise velocity evolves longitudinally and becomes approximately self-similar between x=7 m and x=8 m where the universal log-law fits the measurements. At the most downstream cross-section, the influence of the downstream gates is observed. Keeping in mind that a compound channel flow is being analysed, some influence of 3D turbulence is expected in the centre of the channel. Therefore, other small discrepancies are ascribable to the interaction between main channel and floodplain flows. Despite that, a good agreement with the logarithmic-law profile is observed.

According to Schlichting (1968), the boundary layer thickness in turbulent flow, $\delta\prime$, may be defined by $\delta\prime/x = 0.37(U_\infty\,x/\nu\,)^{-1/5}$ where, U_∞ is the external flow stream velocity. In the case of open channel flows, U_∞ is frequently replaced by the free surface flow velocity, which, in turn, is practically equal to the maximum flow velocity of a given profile.

Note that the cross-section x=0 m is located at the end of the splitting plate between the main channel and the floodplain but the channel starts approximately 1 m upstream and therefore the development of boundary layer starts at $x = -1.0$. Applying the previous equation to the present flow conditions, it may be concluded that at x=7.5 m the boundary layer thickness should be approximately 0.145 m (ν = 1.2×10^{-6} m^2s^{-1} for water at 15°) and it will extend over the whole flow depth. Comparing the calculated boundary layer thickness with the main channel flow depth (h_{mc} = 0.1402 m), it seems reasonable to assume that the

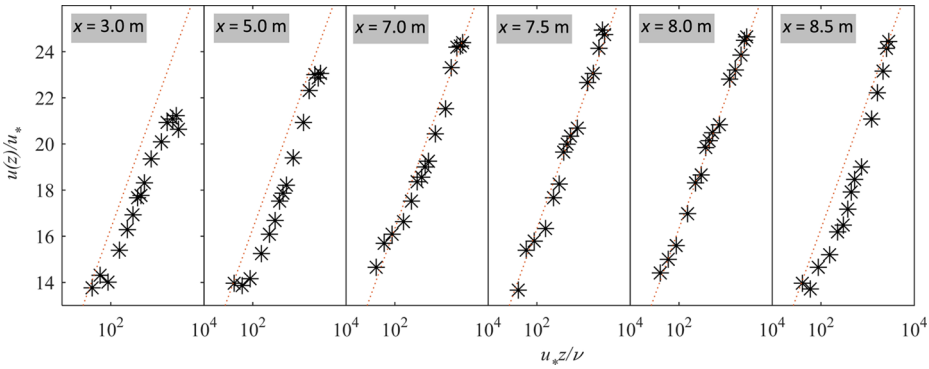

Fig. 2 Vertical profiles of the streamwise velocity in the centre of the channel for flow hr30s

boundary layer occupies the entire flow depth at $x=7.5$ m. The same is true for the remaining flow cases characterized in Table 1.

3.2 Shear Layer

Due to the change on the flow depth between main channel and floodplain, streamwise velocities will have lateral variations in compound channels and a shear layer is observed in the interface between the subsections. The longitudinal development of the flow and shear layer in compound channels was assessed for the 6 uniform flow experiments, namely, flow cases hr015s, hr015r, hr020s, hr020r, hr030s and hr030r. For these flow cases, measurements were conducted at cross-sections $x=1.1$ m, 3 m, 5 m and 7.5 m (cf. Table 1).

The streamwise velocity, $\overline{u}$, scaled by the cross-section averaged streamwise velocity, U_{ave}, is shown in Fig. 3 where y stands for the lateral distance to the main channel centre and z for the vertical distance to the main channel bottom.

The streamwise velocity distribution in the four cross-sections reveals, for all flow cases, the longitudinal development of the boundary layer and the mixing layer. As mentioned before, the former may be recognized for instance in the region near the centre of the channel ($y\approx 0$ m), by the velocity difference which extends until the last two cross-sections, $x=5.0$ m and $x=7.5$ m.

The development of the interaction between the flows in the main channel and in the floodplains is particularly evident in flow case hr015r. From $x=3.0$ m to $x=7.5$ m, the streamwise velocity in the main channel decreases due to the interaction with the slower floodplain flow. This effect leads to a distortion of the isovels, especially in the region above the bankfull level where the influence of the floodplain flow is mainly observed. The opposite effect is observed in the floodplain flow. Along the longitudinal direction, floodplain flow near the interface is accelerated due to the interaction with the main channel flow.

The main driving factor for the mixing layer generation is the gradient of the streamwise velocities in the two subsections (e.g. Dupuis et al. 2017). Defining U_h and U_l as the depth-averaged velocities outside of a mixing layer, in the regions of higher and lower velocities, respectively, the following three characteristic parameters may be defined: (i) characteristic convection velocity of the mixing layer, $U_c = (U_h + U_l)\ /2$; (ii) the charac-

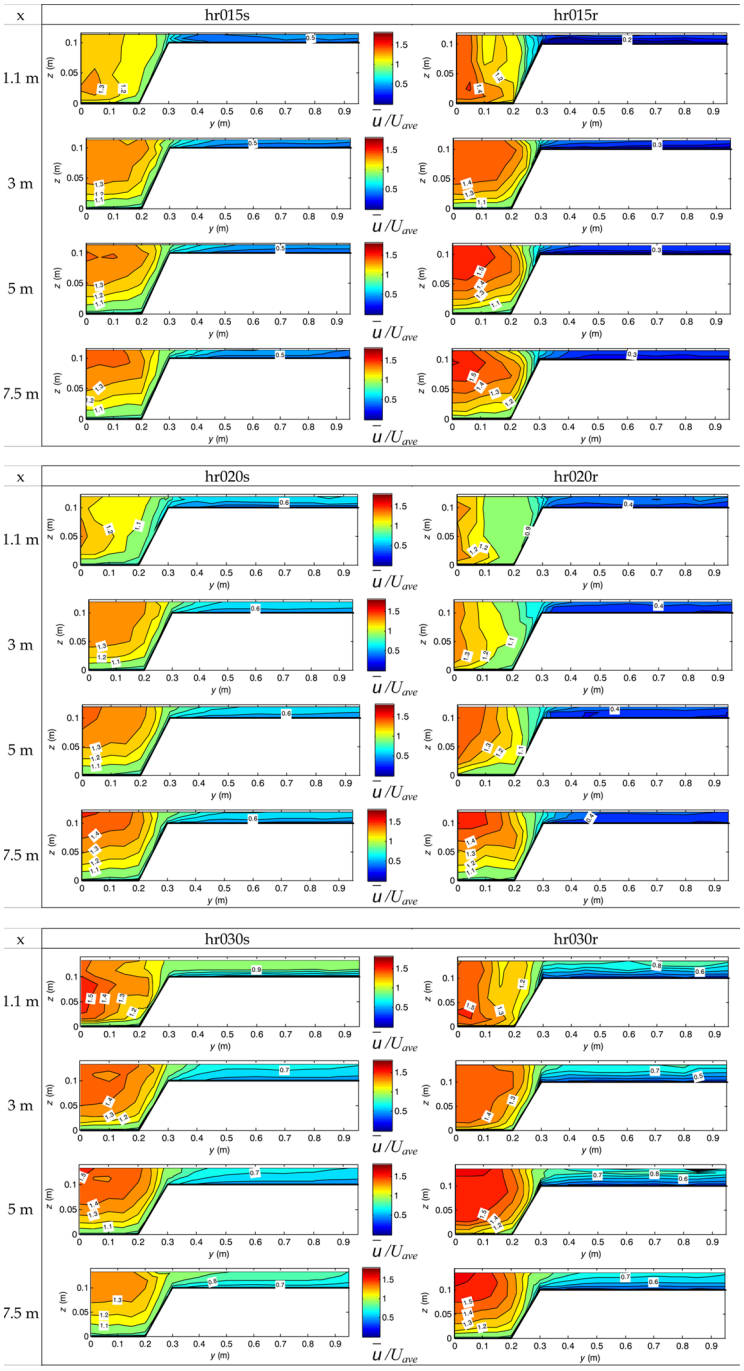

Fig. 3 Cross-section distribution of the streamwise velocity along the compound channel

teristic velocity difference, $U_s = U_h - U_l$ and (iii) the characteristic mixing layer parameter, $\lambda_{ml} = (U_h - U_l)/(U_h + U_l)$.

According to Champagne et al. (1976), the longitudinal spreading rate parameter can be defined as $S_p = U_c/U_s \mathrm{d}\delta/\mathrm{d}x$ where δ is the mixing layer width and therefore $\mathrm{d}\delta/\mathrm{d}x$ is the longitudinal spreading of the mixing layer width. In the case of free mixing layers, without any boundary confinement the longitudinal spreading rate parameter must be constant according to Pope (2000). Values of S_p equal to 0.097 or ranging from 0.06 to 0.11 were reported in the literature. The variation in the measured values of S_p in the literature from one experiment to another is partly attributed to the state of the flow leaving the splitter plate (e.g. Slessor et al. 1998).

In the case of compound channel flows, mixing layer width can be defined using different criteria. Figure 4(a) presents the criterion defined by Pope (2000), where the lateral position y_α can be indirectly determined using $U_{y_\alpha} = U_h + \alpha U_s$ (for $0 < \alpha < 1$). The definitions of $U_{0.1}$, $U_{0.9}$, $y_{0.1}$ and $y_{0.9}$ are schematically presented for a typical depth-averaged streamwise velocity profile of a compound channel flow. Pope (2000) defined the mixing layer width, δ, as the difference between positions $y_{0.1}$ and $y_{0.9}$, i.e., $\delta = |y_{0.9} - y_{0.1}|$, and van Prooijen et al. (2005) used the equation $\delta = 2|y_{0.75} - y_{0.25}|$.

The longitudinal variation of the mixing layer width, δ, derived from the depth-averaged velocity measurements is presented in Fig. 4(b). The spreading rates of δ, $S_p = 0.06$ and $S_p = 0.11$ are also included.

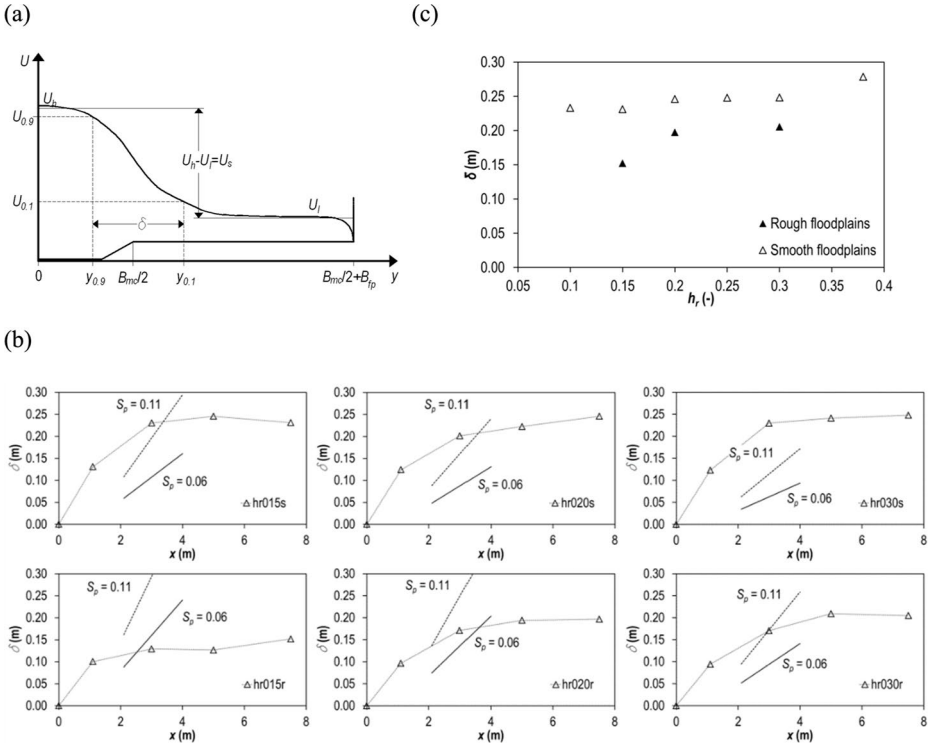

Fig. 4 Mixing layer (**a**) Definitions (criterion defined by Pope 2000). (**b**) Longitudinal evolution of the mixing layer width and (**c**) mixing layer width for the experimental data of the present study

The width of the mixing layer increases along the longitudinal direction from upstream to downstream. This pattern is accompanied by the occurrence of advected turbulent eddies and a maximum turbulence along this mixing layer due to the increased shear and velocity gradient (cf. Han et al. 2016).

In the upstream reach of the compound channel ($x<1.1$ m), the mixing layer develops with spreading rates similar to those of plane mixing layers. Higher growth rates are observed for flow cases on smooth floodplains. Due to the effect of the additional friction caused by the bottom wall, a decrease in the growth rate can be observed between the second and the third cross-sections, $x=3.0$ m and $x=5.0$ m and further downstream. Similar decrease was observed, for instance, by Uijttewaal and Booij (2000), in the development of shallow mixing layers generated by two flows with the same depths but different velocities.

In shallow-water flows, the spreading of the mixing layer is restrained by the additional friction due to the bottom. Additionally, in such flows, there is a geometrical restriction of the water motion and eddies larger than the water depth cannot move or stretch in the vertical direction. For flow cases with the same relative depth but different floodplain roughness the development of the mixing layer is slower for rough floodplain.

The lateral shear stresses were also obtained from the velocity measurements. The longitudinal evolution of the lateral shear stress in the vertical plane, $-\rho\,\overline{u\prime\,v\prime}$, is presented in Fig. 5.

The magnitude of the lateral shear stress increases along the longitudinal direction. Due to the higher velocity gradient between the flows in each subsection, it was found that the roughness in the floodplains enhances the lateral shear stress near the interface between the main channel and the floodplain. For all flow cases, the turbulent shear layer spreads laterally towards the main channel and floodplain in the downstream direction.

The highest shear regions and the peaks of lateral shear stress are located close to the main channel edge. This region is located in the same lateral position (approximately $y=0.28$ m) for almost all flow cases and longitudinal cross-sections. This position falls close to the location of the centre of the mixing layer, $y_{0.5}$ (definition on Fig. 4a).

4 Developed Flows in Compound Channels

4.1 Turbulent Flow Structure

From the previous results it seems reasonable to consider that, with the exception of hr038s, the mixing layer and the boundary layer are fully developed for all flow cases in the cross-section located at $x=7.5$ m. The present analysis of the developed flow in compound channels will be performed for that cross-section. The time-averaged streamwise velocity distributions, $\overline{u}$, at that cross-section are presented in Fig. 6 for the nine uniform flow cases. The same figure (right column) shows the depth-averaged streamwise velocity, U, which writes $U = \frac{1}{H}\int_0^H \overline{u}dz$.

In both cases, velocity distributions are scaled by the averaged cross-section streamwise velocity, U_{ave}.

The streamwise velocity distribution is strongly influenced by the relative depth and the roughness of the floodplains.

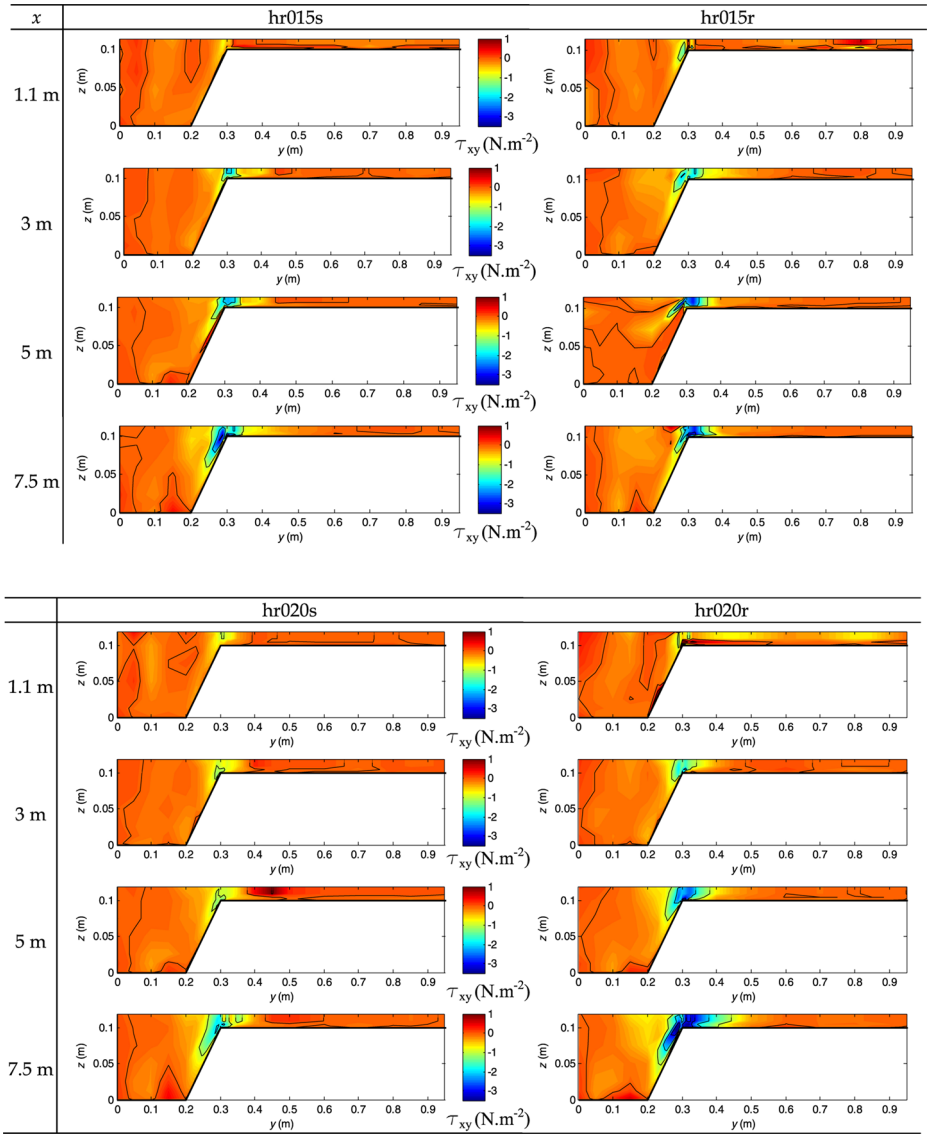

Fig. 5 Cross-section distribution of the lateral shear stress along the compound channel

The curvature of the isovels in the main channel towards its centre is observed for smaller relative depths. This effect is induced by the slower floodplain flow and it is enhanced in the flow cases with rough floodplains. The roughness of the floodplains not only reduces the velocity in the floodplains but it strongly affects the main channel flow. It highlights the mixing between the flows in the main channel and in the floodplain and it is in accordance with the results of Nezu et al. (1999) for relative depths bellow 0.33.

With the increase of the relative depth, the isovels in the main channel become closer to what can be observed in a single trapezoidal channel.

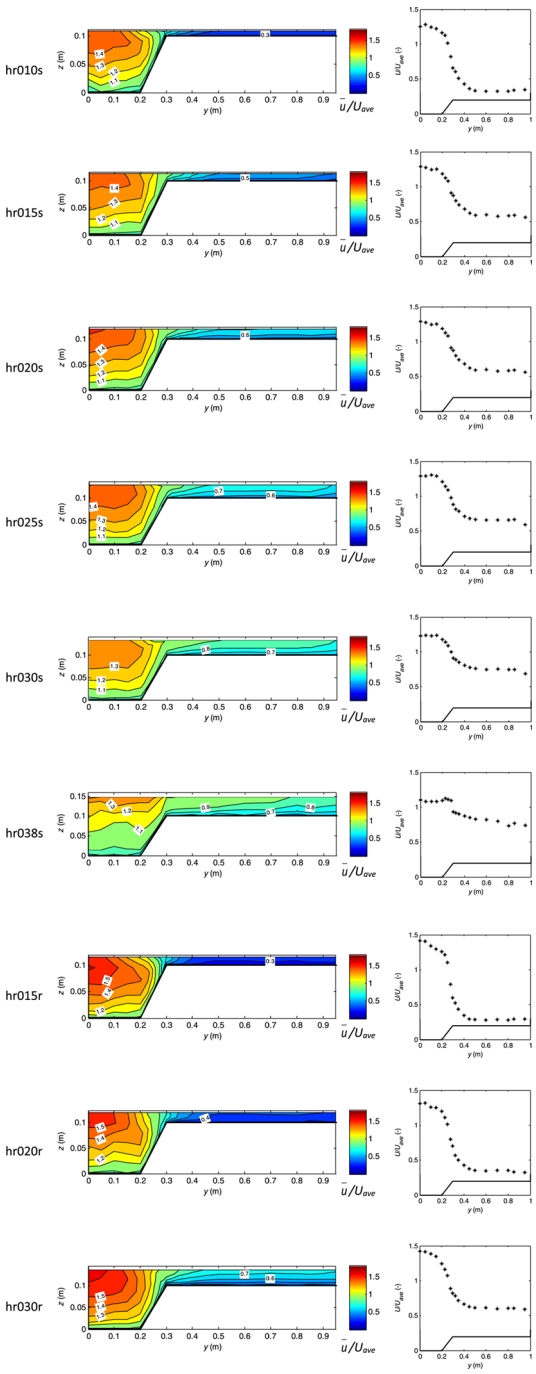

Fig. 6 Time-averaged streamwise velocity, $\overline{\mathrm{u}}$, and depth-averaged streamwise velocity, U , scaled by the cross-section averaged streamwise velocity, U_{ave}, in cross-section $x = 7.5$ m

It is observed that the isovels do not bulge upward near the interface, suggesting that the secondary currents are not strong enough to influence the streamwise velocity distribution.

Regarding the depth-averaged streamwise velocity, the floodplain is wide enough for the establishment of a constant value in the depth-averaged streamwise velocity.

The reduction of the velocity gradient between main channel and floodplain flows with the increase of the relative depth is observed. On contrary, rough floodplains lead to an increase in the velocity gradient.

Figure 7 presents the distribution of the time-averaged lateral shear stress in the cross-section $x = 7.5$ m for the nine flow cases under uniform flow. In the same figure (right column) the lateral distributions of the depth-averaged lateral shear stress, $\tau_{xy}^{d} = \frac{1}{H}\int_{0}^{H}\left(-\rho\,\overline{u'v'}\right)\mathrm{d}z$, are also presented.

The results of the cross-section distribution of lateral shear stress show the influence of the interaction between the main channel and the floodplains flows. The depth-averaged lateral shear stress is approximately equal to zero far from the interface ($y < 0.2$ m and $y > 0.4$–0.5 m). The shear layer is observed for the region $0.2\ \mathrm{m} < y < 0.4$–$0.5$ m. In this region, the lateral profile features a bell shape previously identified, for instance, in Juez et al. (2019). The absolute value of the lateral shear stress increases rapidly, reaching a peak in the main channel near the interface ($y \approx 0.28$–0.30 m). The region of higher shear spreads laterally from this lateral position ($y \approx 0.30$) towards the main channel and the floodplain. It also expands vertically towards the main channel bank.

The lateral shear stress is related with the gradient of the streamwise velocity. With the increase of the relative depth, the gradient decreases and the lateral shear stress in the interface follows this decrease. The same pattern is observed in the experiments with rough floodplains, where the lateral shear stress is enhanced near the interface.

4.2 Mixing Layer and Coherent Flow Structures

The mixing layer widths calculated for the fully developed flows were previously shown in Fig. 4(c). The position of the mixing layer in the region of higher velocity (definition in Fig. 4a), $y_{0.9}$, is located approximately over the beginning of the main channel bank for all flow cases. The limit of the mixing layer in the region of lowest velocity, $y_{0.1}$, shows a slightly increase with the relative depth for flow cases with smooth floodplains. For the rough floodplains flow cases, $y_{0.1}$ is closer to the interface than in the flow cases with smooth floodplains, and no clear influence of the relative depth is observed. In accordance with the results presented by Juez et al. (2019), for flow cases with floodplains covered by synthetic grass, the mixing layer width is smaller than for smooth floodplains. It is observed that this difference is attenuated with the increase of the relative depth, due to the decrease of the roughness influence.

The interaction between the flows in the main channel and in the floodplain generates a shear layer around the interface. This region is characterized by the occurrence of coherent structures with vertical axis characterized by strong vorticity concentration that induce a local roll-up of the flow and keep a characteristic shape during a certain time scale (Lesieur 2008). For the current uniform flow cases, the characteristics of these coherent structures in the shear layer may be influenced by both the roughness of the floodplain and the relative flow depth. The existence of these coherent structures makes easier the momentum transfers

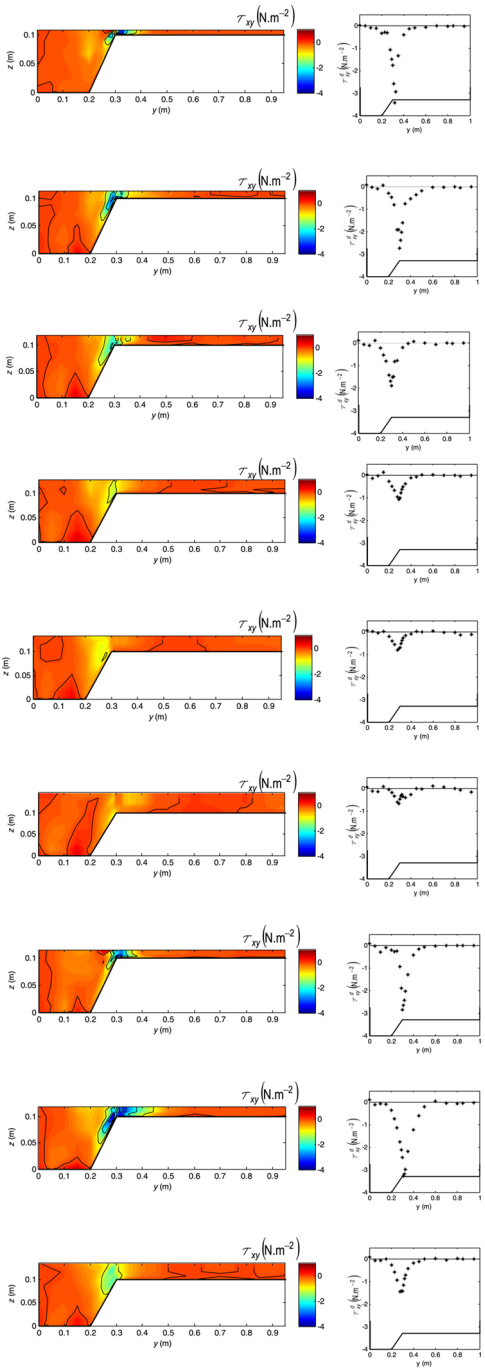

Fig. 7 Distributions of the lateral shear stress and of the depth-averaged lateral shear stress in cross-section $x = 7.5$ m

by turbulent mixing between main channel and floodplain flows and may influence the mixing layer width in the interface (e.g. Jirka 2001).

The identification of the 2D coherent structures may be based on the two types of 2D turbulence (e.g. Proust et al. 2017). The first type stands for a purely 2D isotropic turbulence, forced at a wave number k and without vortex stretching. It is a freely decaying turbulence presenting an energy spectrum with a double cascade. In the power density spectra of the fluctuation velocities, these structures are identified by the $k^{-5/3}$ spectrum from large to small k-wave numbers, i.e., from small to large scales followed by the k^{-3} range (high k-values). In the second type of 2D coherent structures, vortex stretching may be observed. These structures were identified by Stocchino and Brocchini (2010) in a compound channel. Besides the cascade with a $k^{-5/3}$ spectrum, an energy peak in the power spectra is then also observed.

The coherent structures can be identified from the streamwise and spanwise velocity time series, namely by the periodic oscillation of these velocities around the time-averaged value. In this work, these oscillations were inferred by the autocorrelation function, R, and the power density spectra, S, for velocity fluctuations.

The autocorrelation function of the spanwise velocity fluctuations, R_{yy}, over a time span, $\triangle t$, is (e.g. Pope 2000): : $\mathrm{R_{yy}} = \frac{\mathrm{v'(t)v'(t+\backslash varDelta\,t)}}{\overline{\mathrm{v'(t)^2}}}$.

Autocorrelation functions and wavenumber power spectra of the spanwise fluctuation velocities are presented in Fig. 8 for the point located at the interface between the main channel and floodplain flows at 40% of the flow depth for flow cases hr015s, hr020s, hr030s, hr015r, hr020r and hr030r. The wave number, k, was calculated using the streamwise velocity $k = 2\pi F/\overline{\mathrm{u}}$, where F is the frequency.

The integral flow scales may be used to derive the size, shape and travelling times of turbulent vortical structures and its determination is an objective for both fundamental research and practical applications (e.g. Tropea et al. 2007).

The Eulerian integral time scales of spanwise velocity fluctuations, τ_{yy}, may be obtained from the autocorrelation function as (e.g. Nikora et al. 1994), $\tau_{yy} = \int_0^{\infty} R_{yy}(t)\,dt$

Following the procedure of Dupuis et al. (2017), the Eulerian integral time scales of the spanwise velocity fluctuations were calculated from the autocorrelation functions and taken as four times the first zero-crossing.

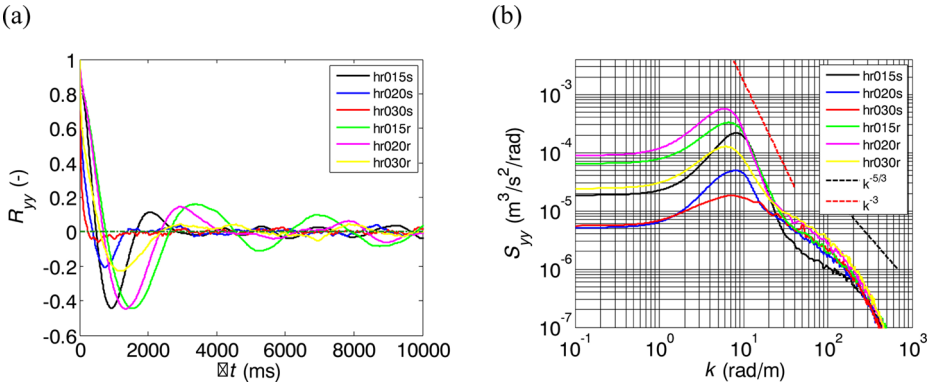

Fig. 8 (**a**) Autocorrelation functions of spanwise velocity fluctuations and (**b**) cross-power spectra density for spanwise velocity fluctuations.

For steady and uniform turbulent flow, using Taylor's hypothesis for the integral length scale for the spanwise turbulent length scale $\Lambda_{yy} = \tau_{yy}.U_c$ where U_c is the convection velocity which can be taken as the streamwise depth average velocity at the interface (e.g. Dupuis et al. 2017). For increasing relative depths (from 0.15 to 0.3), the results obtained for the spanwise turbulent length scales were from 0.9 to 0.5 m for smooth floodplain and from 1.04 to 0.81 m for vegetated floodplains.

For all cases, the power spectra density of the spanwise velocity fluctuations (Fig. 8b) show a typical profile comprising a peak region near a frequency of 0.5 Hz. The 2D characteristic of the large coherent structures may be recognized by the slope of approximately k^{-3} in the middle range of the energy spectra of the turbulence (e.g. Uittewall and Booij 2000). The large coherent structures may also be identified by the modulation of the autocorrelation functions in a clear correspondence to the peaks of the power density spectra. In this type of flow, bottom turbulence may be neglected in regard to the shear layer turbulence. For higher frequencies, the inertial range is recognized by the slope $k^{-5/3}$.

Apart from this general pattern, some differences among the uniform flow cases are observed. For small relative depths, a strong modulation in the autocorrelation functions in the spanwise velocity fluctuations reveals the presence of large coherent structures. Turbulent structures of flow for these shallower flows are coherent over a much longer duration. With the increase of the relative depth, these large structures tend to vanish and only small-scale turbulence is observed. For the same relative depths, with the increase of the roughness a higher magnitude of the peak in the power density spectra is observed suggesting that floodplain vegetation enhances the formation of the larger scale coherent structures.

It is noted that higher relative depth and smooth floodplain (hr03s) lead to much less shear and the 2D coherent structures almost vanish. This is identified by the reduction of the peak in the power density spectra.

Comparing flow cases with similar flow depth but different floodplain roughness it is clear that floodplain vegetation enhances the occurrence of large-scale coherent structures. In accordance with Truong et al. (2019) and Juez et al. (2019), the presence of vegetation seems to be the dominant factor controlling the dynamics of the mixing layer.

5 Conclusions

The typical configuration of rivers in alluvial reaches is a compound channel where flows with different depths and velocities interact forming a mixing and shear region near the interface between main channel and floodplains. The complexity associated to these flows leads to difficulties in the prediction of the total conveyance and of the discharge distribution between the subsections. Due to the intermittent inundation of the floodplains, these regions are usually vegetated with the associated change of roughness.

In the present paper, the streamwise development and the fully developed overbank flows in with and without vegetation were investigated by means of acoustic velocity measurements in a compound channel. The experiments comprised six uniform flows with smooth floodplains and three uniform flows with floodplains covered with synthetic grass.

Velocity measurements in the centre of the main channel for one flow case revealed the fully development of the boundary layer in the Sect. 7.5 m from the inlet.

The roughness of the floodplains not only reduces the velocity in the floodplains but it strongly affects the main channel flow. The slower flow in the floodplain influences the flow in the main channel above the bankfull level. The velocity gradient of the flows in these subsections is the trigger for the generation of the mixing layer. Following the upstream reach where the spreading rate of the mixing layer width is similar to a free mixing layer, it is restrained by the additional friction due to the bottom. For flow cases with the same water depth and different floodplain roughness, a higher growth rate is observed for flows on smoother floodplains while a constant mixing layer width is achieved further from the inlet section.

The shear layer is characterized by high values of lateral shear stress in the interface. It is enhanced by the floodplain roughness and the lower relative depths. The peaks of lateral shear stress correspond to the centre of the mixing layers. The region of higher shear spreads laterally from this lateral position towards the main channel and the floodplain. It also expands vertically towards the main channel bank.

Author Contributions All authors contributed to the study's conception and design. Material preparation, data collection, and analysis were performed by João N.S. Fernandes. The first draft of the manuscript was written by João N.S. Fernandes and all authors commented on previous versions of the manuscript. All authors read and approved the final manuscript.

Funding This work was done with the support of FEDER and Science and Technology Foundation under the scope of the Project MixFluv – Mixing Layers in fluvial systems (PTDC/ECI-EGC/31771/2017).

Data Availability The data that support the findings of this study are available from the corresponding author, J.N.F., upon reasonable request.

Declarations

Ethical Approval Not applicable.

Consent to Participate Not applicable.

Consent to Publish Not applicable.

Competing Interests The authors have no relevant financial or non-financial interests to disclose.

References

Booij R, Tukker J (2001) Integral model of shallow mixing layers. J Hydraul Res 39(2):169–179

Bousmar D, Rivière N, Proust S, Paquier A, Morel R, Zech Y (2005) Upstream discharge distribution in compound-channel flumes. J Hydraul Eng 131(5):408–412

Bousmar D, Mathurin B, Fernandes JN, Filonovich M, Hazlewood C, Huthoff F, Proust S (2016) Uniform flow in prismatic compound channel: Benchmarking numerical models. In: River Flow - Proceedings of the International Conference on Fluvial Hydraulics. St. Louis, USA, pp 272–280. https://doi.org/10.1201/9781315644479-46

Champagne FH, Pao YH, Wygnanski IJ (1976) On the two-dimensional mixing region. J Fluid Mech 74(2):209–250

Chu VH, Wu JH, Khayat RE (1991) Stability of transverse shear flows in shallow open channels. J Hydraul Eng 117(10):1370–1388

Dupuis S, Proust S, Berni S, Paquier A (2017) Compound channel flow with a longitudinal transition in hydraulic roughness over the floodplains. Environ Fluid Mech 17:903–928. https://doi.org/10.1007/s10652-017-9525-0

Fernandes J, Leal J, Cardoso A (2018) Influence of floodplain and riparian vegetation in the conveyance and structure of turbulent flow in compound channels. In: River Flow 2018–9th Int Conf Fluvial Hydraulics, vol 40. E3S Web of Conferences, EDP Sciences, pp 8. https://doi.org/10.1051/e3sconf/20184006035
Goring DG, Nikora VI (2002) Despiking acoustic Doppler velocimeter records. J Hydraul Eng 128(1):117–126
Han L, Mignot E, Rivière N (2016) Shallow mixing layer downstream from a sudden expansion. J Hydraul Eng 143(5). https://doi.org/10.1061/(asce)hy.1943-7900.0001274
Jirka GH (2001) Large scale flow structures and mixing processes in shallow flows. J Hydraul Eng 39(6):567–573. https://doi.org/10.1080/00221686.2001.9628285
Juez C, Schärer C, Jenny H, Schleiss AJ, Franca MJ (2019) Floodplain land cover and flow hydrodynamic control of overbank sedimentation in compound channel flows. Water Resour Res 55(11):9072–9091
Lesieur, M. (2008). Turbulence in fluids. In: Fluid mechanics and its applications. Springer. https://doi.org/10.1007/978-1-4020-6435-7
Myers WR, Lyness JF (1994) Hydraulic study of a two-stage river channel. Regul Rivers Res Manag 9(4):225–235. https://doi.org/10.1002/rrr.3450090404
Nezu I, Onitsuka K, Iketani K (1999) Coherent horizontal vortices in compound open channel flows. In: Seo IW, Singh VP, Sonu JH (eds) Hydraulic modeling. Water Resources, Colorado, USA, pp 17–32
Nikora VI, Rowiski P, Sukhodolov A, Krasuski D (1994) Structure of river turbulence behind warm-water discharge. J Hydraul Eng 120(2):191–208. https://doi.org/10.1061/(ASCE)0733-9429(1994)120:2(191)
Pope SB (2000) Turbulent flows. Cambridge University Press
Prasad P B.S.S., Sharma A, Khatua KK (2022) Distribution and prediction of Boundary Shear in diverging compound channels. Water Resour Manage 2022. https://doi.org/10.1007/s11269-022-03286-y
Proust S, Berni C, Boudou M, Chiaverini A, Dupuis V, Faure JB, Paquier A et al (2016) Predicting the flow on the floodplains with evolving land occupations during extreme flood events (FlowRes ANR project). FLOODrisk (2016). In: 3rd European Conference on Flood Risk Management, Lyon. E3S Web of Conferences. https://doi.org/10.1051/e3sconf/20160704004
Proust S, Fernandes JN, Leal JB, Rivière N, Peltier Y (2017) Mixing layer and coherent structures in compound channel flows: Effects of transverse flow, velocity ratio, and vertical confinement. Water Resour Res 53(4):3387–3406. https://doi.org/10.1002/2016wr019873
Rahimi H, Yuan S, Tang X, Lu C, Singh P, Dehrashid F (2022) Study on Conveyance Coefficient Influenced by Momentum Exchange under steady and unsteady flows in compound open channels. Water Resour Manage 36:2179–2199. https://doi.org/10.1007/s11269-022-03130-3
Schlichting H (1968) Boundary-layer theory, 6th edn. McGraw Hill Book, Co. Inc., New York, U.S.A., p 748
Slessor MD, Bond CL, Dimotakis PE (1998) Turbulent shear-layer mixing at high Reynolds numbers: effects of inflow conditions. J Fluid Mech 376:115–138
Stocchino A, Brocchini M (2010) Horizontal mixing of quasi-uniform straight compound channel flows. J Fluid Mech 643:425–435
Tropea C, Yarin A, Foss JF (2007) Springer Handbook of experimental fluid mechanics. Springer, Berlin Heidelberg
Truong SH, Uijttewaal SJ, Stive MJF (2019) Exchange processes induced by large horizontal coherent structures in floodplain vegetated channels. Water Resour Res 55:2014–2032
Uijttewaal WSJ, Booij R (2000) Effects of shallowness on the development of free-surface mixing layers. Phys Fluids 12(2):392–420
van Prooijen BC, Battjes JA, Uijttewaal WSJ (2005) Momentum exchange in straight uniform compound channel flow. J Hydraul Eng (Reston) 131(3):175–183
Vermaas DA, Uijttewaal W, Hoitink AJF (2011) Lateral transfer of streamwise momentum caused by a roughness transition across a shallow channel. Water Resour Res 47:W02530
Vojoudi Mehrabani F, Mohammadi M, Ayyoubzadeh SA, Fernandes JN, Ferreira RML (2020) Turbulent flow structure in a vegetated non-prismatic compound channel. River Res Appl 36(9):1868–1878
Yule AJ (1972) Two-dimensional self-preserving turbulent mixing layers at different free stream velocity ratios, Aeronautical Research Council. Reports and memoranda. Department of the Mechanics of Fluids, University of Manchester. https://reports.aerade.cranfield.ac.uk/handle/1826.2/2957
Zeng YH, Guymer I, Spence KJ, Huai WX (2012) Application of analytical solutions in trapezoidal compound channel flow. River Res Appl 28:53–61